CRICK, F. H. & MAGDOFF, B. (1956). *Acta Cryst.* **9**, 901–908.
FORTIER, S., WEEKS, C. M. & HAUPTMAN, H. (1984). *Acta Cryst.* A**40**, 544–548.
GIACOVAZZO, C., CASCARANO, G. & ZHENG C. (1988). *Acta Cryst.* A**44**, 45–51.
GIACOVAZZO, C., GUAGLIARDI, A., RAVELLI, R. & SILIQI, D. (1994). *Z. Kristallogr.* **209**, 136–142.
GIACOVAZZO, C., SILIQI, D. & RALPH, A. (1994). *Acta Cryst.* A**50**, 503–510.
GIACOVAZZO, C., SILIQI, D. & SPAGNA, A. (1994). *Acta Cryst.* A**50**, 609–621.
GLOVER, I., HANEEF, I., PITTS, J., WOODS, S., MOSS, D., TICKLE, I. & BLUNDELL, T. L. (1983). *Biopolyers*, **22**, 293–304.
HAUPTMAN, H. (1982). *Acta Cryst.* A**38**, 289–294.
JONES, T. A. (1978). *J. Appl. Cryst.* **11**, 268–272.
JONES, T. A., ZOU, J.-Z., COWAN, S. W. & KJELDGAARD, M. (1991). *Acta Cryst.* A**47**, 110–119.
KRETSINGER, R. H. & NOCKOLDS, C. E. (1973). *J. Biol. Chem.* **248**, 3313–3326.
KYRIAKIDIS, C. K., PESCHAR, R. & SCHENK, H. (1993). *Acta Cryst.* A**49**, 350–358.
MATTEVI, A., OBMOLOVA, G., SCHULZE, E., KALK, K. H., WESTPHAL, A. H., DE KOK, A. & HOL, W. G. J. (1992). *Science*, **255**, 1544–1550.
ZANOTTI, G., SCAPIN, G., SPADON, P., VEERKAMP, J. H. & SACCHETTINI, J. C. (1992). *J. Biol. Chem.* **267**, 18541–18550.

Acta Cryst. (1995). A**51**, 188–197

The Estimation of Crystal Thickness and the Restoration of Structure-Factor Modulus from Electron Diffraction: a Kinematical Approach

BY D. TANG, J. JANSEN AND H. W. ZANDBERGEN

National Centre for HREM, Laboratory of Materials Science, Delft University of Technology, Rotterdamseweg 137, 2628 *AL Delft, The Netherlands*

AND H. SCHENK

Laboratory for Crystallography, University of Amsterdam, Nieuwe Achtergracht 166, 1018 *WV Amsterdam, The Netherlands*

(*Received* 6 *April* 1994; *accepted* 8 *September* 1994)

Abstract

A technique of crystal-thickness estimation and structure-factor-modulus restoration (reconstruction) from electron diffraction patterns, for use in crystal-structure determination, is proposed based on the kinematic scattering theory. A criterion for a self-consistent test of the restored structure-factor modulus has also been introduced from the structure-factor statistics developed by direct methods for X-ray diffraction. Theoretical tests on some structures are successful and show that the diffraction intensities are improved to be closer to the moduli of the true structure factors.

1. Introduction

The techniques of combined high-resolution electron microscopy (HREM) with electron diffraction intensity have been used for both HREM image deconvolution and resolution enhancement (*e.g.* Ishizuka, Miyazaki & Uyeda, 1982; Fan, Zhong, Zheng & Li, 1985; Liu *et al.*, 1990; Downing, Meisheng, Wenk & O'Keefe, 1990; Dong *et al.*, 1992; Hu, Fan & Li, 1992; Zou, Hovmöller, Parras, González-Calbet, Vallet-Regí & Grenier, 1993). These techniques are very useful in cases when crystals are too small for X-ray or neutron diffraction. Nearly all of these studies were for the kinematical condition (weak-phase-object approximation) or near the kinematical condition (pseudo-weak-phase-object approximation) (Tang & Li, 1988), that is when electron dynamical scattering is not predominant. Under such conditions, the phase of the diffracted wave function is replaced by the phase of the Fourier transform of the corresponding high-resolution electron-microscope image so that the phase problem that occurs in X-ray diffraction can be partly resolved.

Although the dynamical-diffraction effect is much stronger in electron diffraction than in X-ray diffraction, the dynamical perturbations to the diffracted beams are expressed as phase distortions before the wave amplitudes change much from their kinematical values (Dorset, Tivol & Turner, 1992). That is to say, the electron diffraction intensity is proportional to the square of the modulus of the structure factor in a greater range of thickness than that for which kinematical diffraction is valid.

A well known formula for the kinematical diffracted intensity, neglecting the Lorentz–polarization correction, gives the relative intensity as (Vainshtein, 1964; Cowley, 1988)

$$I(\mathbf{g}) = |F(\mathbf{g})|^2[(\sin \pi s_g t)/\pi s_g t]^2. \quad (1)$$

©1995 International Union of Crystallography
Printed in Great Britain – all rights reserved

Here, t is the specimen thickness, $\mathbf{g}$ is a reciprocal vector, $F(\mathbf{g})$ is the structure factor, s_g is called the excitation error, which is equivalent to the distance from the Ewald-sphere surface to the reciprocal lattice (see Fig. 1). The shape function $D(s, t) = (\sin \pi s_g t)/\pi s_g t$ has a principal maximum of unity. Fig. 2 shows how the square of the shape function, $D^2(x)$, varies with its argument x. It is worth mentioning that for (1) the incident electron beam is assumed to be parallel and the specimen is assumed to have an infinite-slice shape in the lateral directions so that the diffraction spot is a geometrical point. In experimental work, this is never true and the intensity is distributed around each diffraction spot. Therefore, the measured intensity value on the left-hand side of (1) should be the integrated intensity.

In the past, the curvature of the scattering sphere or the Ewald sphere, which introduces the shape function, is generally ignored while collecting electron diffracted intensities either by a microdensitometer or a CCD (charge-coupled device) camera (Baldwin & Henderson, 1984; Zou, Sukharev & Hovmöller, 1993). Because the electron wavelength λ is very short (0.01 Å compared with 1 Å for X-rays), the radius of the sphere is so large that sometimes it is a very good approximation to treat the spherical surface as a plane. For example, at 300 kV, the spherical radius is more than 50 $Å^{-1}$, 50 times the maximum spatial frequency of the best modern microscope (1.0 Å resolution). Therefore, it seems unnecessary to involve any other 'scattering surfaces' than a 'scattering plane', so the right-hand side of (1) is simplified to be just the modulus squared of the structure factor. However, at large reciprocal vector length, when the crystal is relatively thick, when the Laue circle is not centred, when the specimen is not correctly oriented, when the incident beam is tilted *etc.*, this is an over-simplification.

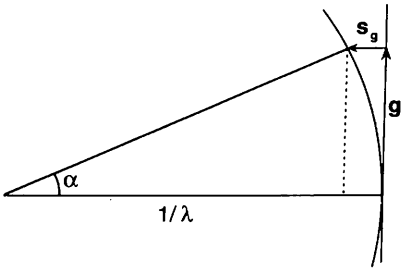

Fig. 1. A schematic diagram showing the propagation of an electron wave in reciprocal space and in real space ($1/\lambda$ replaced by the slice thickness Δz).

For a precise investigation of the structure, especially if the techniques involved depend on the measured diffracted intensities, such as electron direct methods (Dorset, 1992), it will be absolutely necessary to evaluate the diffraction data with great care. A small beam spot should be used to ensure that the illuminated crystal is almost flat; the crystal should be thin enough to use kinematical diffraction theory; the curvature of the Ewald sphere should be taken into consideration. To correct for this curvature, the crystal thickness should be determined. Pinsker (1953) introduced a method to determine the thickness from the size of the Laue zones. In our opinion, its accuracy is in doubt for a normal-size inorganic unit cell since only the zero-order Laue zone is observable in a principal orientation. However, the shape function included in (1) also gives us a chance to extract a value of the thickness since, in a simple mathematical relationship, the diffraction intensity and the structure factor are connected by a factor containing crystal thickness information.

The value of g, which gives $D^2(s_g t) = 80\%$ or $s_g t = 0.2575$ at 300 kV, is plotted against the crystal thickness in Fig. 3. The figure clearly shows that the deviation of the diffraction intensity from the pure modulus squared of the structure factor is, in principle, negligible when the crystal thickness is less than 25 Å because all the reflections, which are modified by a factor of less than 0.8, locate outside a circle of 1.0 $Å^{-1}$ in reciprocal space, the best image-mode-information limit of a modern electron microscope. However, when the crystal is thick, there will be some reflections having intensities less than 80% of the square of the structure factor, so that the effect of the curvature of the Ewald sphere becomes important and can no longer be ignored.

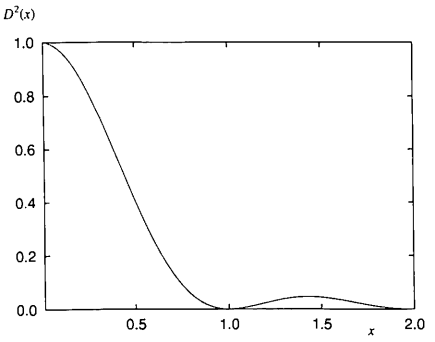

Fig. 2. The square of a shape function $D^2(x)$.

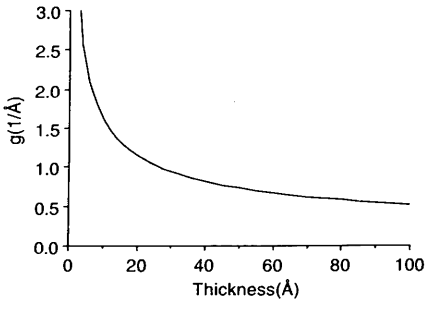

Fig. 3. g values that produce $D^2(s_g t) = 80\%$ *versus* thickness t at 300 kV.

In this paper, the accuracy of diffraction simulation with a paraboloidal scattering surface, which is normally used in the conventional simulation program, is first discussed. The possibility of using (1) and the curvature of the scattering sphere to obtain a set of structure-factor moduli from the diffraction intensities is then investigated. The thickness information hidden in the diffraction data by the shape function is extracted from the diffraction with the help of structure-factor statistics. Starting from the theoretical simulated diffraction intensities, tests on several structures show that a better set of data, which is closer to the structure-factor moduli, can be obtained.

2. The zero and first-order front Fresnel propagator

In the multislice algorithm for diffraction calculation (Cowley & Moodie, 1957; Goodman & Moodie, 1974), the effect of the Ewald sphere is implied in the Fresnel propagator, which describes the wave propagation for a distance of Δz, the thickness of a single slice. Apart from the near-axis, one of approximations made in obtaining this propagator is that of the paraboloidal approximation to a sphere: the spherical wave front is replaced by a paraboloidal front near the optical axis. This section will discuss the difference between a paraboloidal-wave-front Fresnel propagator (zero-order approximation) and one with a higher-order approximation to a sphere, and then estimate the utility of the paraboloidal approximation in diffraction calculations when the curvature of the Ewald sphere is important.

All calculations for this paper were made using a slice size equal to the length of the crystallographic unit cell.

2.1. *The first-order Fresnel propagator*

Fig. 1 shows a geometrical construction of the wave propagation in both reciprocal space and real space. The figure is not drawn to scale since $1/\lambda$ is much larger than any reciprocal vector length g inside the resolution limit of a microscope. The phase difference between the wave travelling with an angle α to the axis and the unscattered beam going through a distance Δz (replacing $1/\lambda$ for real-space display) is

$$\begin{aligned}\Delta\varphi &= (2\pi/\lambda)(\Delta z/\cos\alpha) - (2\pi/\lambda)\Delta z \\ &= (2\pi/\lambda)\Delta z(1/\cos\alpha - 1). \end{aligned} \quad (2)$$

If α corresponds to the direction leading to the end of $\mathbf{g} + \mathbf{s_g}$,

$$\begin{aligned}(\cos\alpha)^{-1} &= (1/\lambda)/(1/\lambda - s_g) \\ &= [1 - (\lambda g)^2]^{-1/2} \\ &= 1 + \tfrac{1}{2}(\lambda g)^2 + \tfrac{3}{8}(\lambda g)^4 + o((\lambda g)^6). \end{aligned} \quad (3)$$

Here, $s_g = (1/\lambda)\{[1 - (\lambda g)^2]^{1/2}\}$ and we suppose $\lambda g << 1$, which is generally true for electron microscopy. For example, at 300 kV and $g_{max} = 1.0\,\text{Å}^{-1}$, the maximum λg is only 0.0197. Hence, we have the first-order Fresnel propagator according to (3) as

$$\begin{aligned}p_1(g) &= \exp(i\Delta\varphi) \\ &= p_o(g)\exp(i\tfrac{3}{4}\pi\Delta z\lambda^3 g^4) \\ &= \exp(i\pi\Delta z\lambda g^2)\exp(i\tfrac{3}{4}\pi\Delta z\lambda^3 g^4). \end{aligned} \quad (4)$$

$p_o(g)$ above is the conventional zero-order Fresnel propagator used in the conventional multislice algorithm, where a sperical wave front is replaced by a paraboloidal one. Since $\lambda^3 g^4$ is very near zero, the first-order propagator is also close to the paraboloidal approximation. The relative phase difference, when the first-order propagator is taken into consideration rather than its inferior one, is equal to $\frac{3}{4}\pi\Delta z\lambda^3 g^4$. Despite the smallness of this phase difference, enhanced by the iteration in the multislice calculation, the diffraction could be different while two kinds of propators are employed.

A similar phase difference has also been obtained by Kilas, O'Keefe & Krishnan (1987) when they estimated the error caused by the excitation error of the higher-order Laue-zone reflection.

2.2. *Tests of the first-order propagator*

The effect of using the first-order Fresnel propagator in a multislice simulation algorithm is assessed by comparing two diffraction functions calculated with the zero and the first Fresnel propagators, respectively. The following tests are based on [010] incidence of $NdSr_2NbCu_2O_8$ (Zandbergen, Cava, Krajewski & Peck, 1993), which has a similar structure to the high-T_c superconductor $YBa_2Cu_3O_{7-x}$ with Nb replacing one of the three copper atoms and $a = b = 3.88$, $c = 11.75$ Å. A voltage of 300 kV ($\lambda = 0.0197$ Å) is employed in this and all other tests throughout the paper. The program for multislice calculation uses the NAG library for the fast Fourier transform. The array size used is 64×32, with sampling distances of 0.18×0.12 Å.

In order to estimate the difference from different calculations, an R factor is introducted, which is defined as

$$R = \sum |I_1^{1/2} - I_2^{1/2}| / \sum I_1^{1/2}, \quad (5)$$

with I_1 and I_2 the intensities at two corresponding pixels from two calculations and the sums over a certain area in reciprocal space, denoted S_{area}. No scaling factor is needed in (5) since diffracted functions are already normalized. To estimate the overall effect of the new propagator, a circular S_{area} will be used while, in order to estimate how R changes in reciprocal space, a series of annular S_{area} is employed instead. S_{area} will be expressed by its radius if the area is a circle or by two radii if it is a ring.

Table 1. *R factors (%) of diffracted amplitudes simulated with zero and first-order Fresnel propagators for* $NdSr_2NbCu_2O_8$ *at various thicknesses and in diverse circular areas*

Thickness (Å)	S_{area} (Å^{-1})					
	0.830	1.174	1.438	1.660	1.856	2.033
19.40	0.009	0.010	0.010	0.015	0.019	0.021
38.80	0.019	0.019	0.024	0.024	0.027	0.031
58.20	0.020	0.023	0.025	0.032	0.034	0.039
77.60	0.016	0.022	0.029	0.034	0.040	0.045
100.88	0.025	0.026	0.030	0.036	0.041	0.046

Table 2. *R factors (%) as in Table* 1, *but calculated in annular areas*

Thickness (Å)	S_{area} (Å^{-1})					
	0.000 0.830	0.830 1.174	1.174 1.438	1.438 1.660	1.660 1.856	1.856 2.033
19.40	0.009	0.011	0.013	0.066	0.113	0.071
38.80	0.019	0.017	0.051	0.030	0.095	0.140
58.20	0.020	0.030	0.037	0.128	0.070	0.200
77.60	0.016	0.042	0.075	0.125	0.214	0.287
100.88	0.025	0.029	0.062	0.121	0.162	0.283

For the annular S_{area}, to make the calculated R values comparable, the areas of individual rings are equal to each other. Mathematically, this implies that the radii are 0 to r_0 (the first area is a circle rather than a ring), r_0 to $2^{1/2}r_0$, $2^{1/2}r_0$ to $3^{1/2}r_0$, $3^{1/2}r_0$ to $4^{1/2}r_0$ *etc.*, making each area equal to πr_0^2. In practice, since the diffracted beams do not uniformly distribute in reciprocal space, the number of reflections in each area will not necessarily be identical. A careful choice of r_0 is important. Too big an r_0 would give the R value averaged over too many beams, which does not precisely represent the relationship of R with the reciprocal-space vector length g. On the other hand, too small an r_0 would lead to R values dominated by the accidental error because of too few reflections in each ring. We accept an available beam number in each ring of about 100, which leads to $r_0 = 0.83$ Å^{-1}.

Diffracted intensities with two propagators $p_0(g)$ and $p_1(g)$ as defined in (4) at five different specimen thicknesses have been computed. The R factors for several S_{area}s are tabulate in Table 1 (circular S_{area}) and Table 2 (annular S_{area}). The general tendency of the R factor changing with both the thickness and the radius of S_{area} is that it increases with an increase in either of them, although there are two exceptions at small radii in Table 1 and the rule is not universal in Table 2. The local variation from the general rule comes partly from the complexity of dynamical scattering and partly from the average over a relatively small number of reflections. It is understandable that the increase of thickness results in the enhancement of the difference by the repeated use of the new propagator, and that the increase of radius in reciprocal space includes (more) beams with larger g values, which in turn makes the deviation bigger. The biggest R factor for the circular S_{area} is 0.046% and that for the annular one is 0.287%, all at thicknesses over 70 Å and with a maximum g over 2.0 Å^{-1}, which are too thick for kinematic scattering and larger than the resolution limit of the microscope.

Considering the small R values even for a very thick specimen and a very large g value, the zero-order paraboloidal approximation to a sphere for the Fresnel propagator is generally a very good approximation, which will not cause any substantial deviation from a higher-order propagator in multislice calculation.

3. Structure-factor restoration

According to (1), under the kinematical condition the diffracted intensity is related to the modulus of the structure factor, and hence it is possible to restore a set of structure-factor moduli from the recorded diffraction intensities. The results of the calculations discussed in §2 indicate that, to a very good approximation, the curvature of the Ewald sphere is properly included in the conventional multislice algorithm by a paraboloidal Fresnel propagator, so that it can be safely used in the theoretical simulation concerning the curvature. In this section, theoretical calculations are performed to test the possibility of restoring a structure factor from a set of diffraction data.

3.1. *Merit factor M*

It is essential to define a merit factor, which should be independent of the investigated structure, thus allowing one to determine the thickness using the reverse of (1):

$$|F(\mathbf{g})|^2 = I(\mathbf{g})/[(\sin \pi s_g t)/\pi s_g t]^2. \tag{6}$$

Putting an arbirary thickness T_{trial} in (6) leads to a set of possible structure-factor moduli $|F'|$. If one set of such $|F'|$s is close to the true structure factor $|F|$, the normalized structure factor $|E'|$ should obey some statistical relationships (see Giacovazzo, 1980). The normalized structure factor is related to the structure factor as

$$|E(\mathbf{g})|^2 = |F(\mathbf{g})|^2 / \sum f_j^2(\mathbf{g}), \tag{7}$$

with f the atomic scattering factor for the jth atom in the unit cell and the sum is over all atoms in the cell. Some statistical averaged values over the whole three-dimensional reciprocal space for both centrosymmetric and noncentrosymmetric structures are given in Table 3. The average is expressed as, for example,

$$\langle |E|^2 \rangle = (1/n) \sum_{j=1}^{n} |E(\mathbf{g}_j)|^2, \tag{8}$$

Table 3. *The normalized structure-factor statistical average values for both centrosymmetric and non-centrosymmetric structures*

	$\|E\|$	$\|E\|^2$	$\|E\|^3$	$\|E\|^4$	$\|E\|^5$	$\|E\|^6$	$\|\|E\|^2-1\|$	$\|\|E\|^2-1\|^2$
Centrosymmetric	0.798	1	1.596	3	6.383	15	0.968	8.691
Non-centrosymmetric	0.886	1	1.329	2	3.323	6	0.736	2.415

with n the number of reflections involved in the calculation, which should be infinite if the space is infinite. In practice, the sum in (8) is rather limited, over a finite areas in reciprocal space (denoted S_{area} again), so that n is a finite number and the average can only be approximated. Theoretical values for the averages differ quite a lot between centro- and non-centrosymmetric space groups, but are almost equal within all the centro- or all non-centrosymmetric space groups. The approximations we use are listed in Table 3 (Giacovazzo, 1980).

Suppose that from energy-dispersive X-ray microanalysis (EDX) or other measurements the element composition of the structure under investigation is known, the 'trial' modulus of the normalized structure factor $|E'|$ can be calculated from $|F'|$ and the above statistical values can then be used as a merit factor to test the closeness of $|F'|$ to $|F|$. The merit factor M is defined as

$$M(T_{\text{trial}}) = \sum_{k=1}^{7} |N'_k(T_{\text{trial}}) - N_k|/N_k, \qquad (9)$$

with the sum over all the statistics in Table 3 except $\langle|E|^2\rangle = 1$, which will be used for the initial normalization. $N'_k(T_{\text{trial}})$ are the statistical values calculated from one set of $|F'|$ using thickness T_{trial} and N_k the expected theoretical values in Table 3. Generally speaking, the smaller $M(T_{\text{trial}})$ is, the closer $|F'|$ is to $|F|$. The minimum $M(T_{\text{trial}})$ is then considered to correspond to the best set of normalized structure factors, the best set of structure-factor moduli and the best trial thickness or the thickness determined T_{det}. The 000 reflection $E(0)$ is not recordable and is set to be zero in all the following tests.

3.2. *S_{area} and thickness limit*

As in the last section, S_{area} is an area in reciprocal space for statistical average calculations. In this section, only circular areas are used. The largest S_{area} is set by the microscope, namely the outermost diffraction intensity that can be recorded, recognized and digitized. From our experience with our Philips CM30-ST-FEG, we know that, along a zone axis, diffraction spots can be observed up to 1.2 Å^{-1} or 0.83 Å resolution in real space. By a double recording technique, it is possible to collect information up to 1.3 Å^{-1} (Zou, Sukharev & Hovmöller, 1993). It is also possible to record diffraction further out by tilting the electron beam and recording several sets of data. Therefore, for a zone-axis diffraction pattern, it is reasonable to chose the largest S_{area} to be 1.2 Å^{-1}.

A larger S_{area} always means more reflections are included in the statistical average, which certainly leads to a better estimation of the closeness of $|F'|$ to $|F|$. However, it should be verified that the thickness is not so great that the denominator in (6) turns out to be very small or $s_g t$ is close to unity. This will result in a huge error and this case should be avoided by setting a thickness limit for a given S_{area} such that $s_g t$ is less than 0.95 or $D(s_g t)$ is always greater than 0.05. For example, because $s_{1.2} = 0.0142$ and $s_{1.0} = 0.0099$ at 300 kV, the corresponding thickness limits are thus about 66 and 96 Å, respectively. All the following tests are performed within the thickness limits for an individual S_{area} according to this criterion.

In all the following tests, starting from $T_{\text{trial}} = 0.0$, the increment of the trial thickness is 2 Å until the limit is reached.

3.3 *Tests of simple structures*

The simple cubic structures of copper, silicon and silicon dioxide (β-cristobalite) (Wells, 1954), along the [001] directions, are used in turn to test the technique of structure-factor restoration from diffraction intensity by the kinematical approach. Because of the small unit cell and the high order of symmetry of these structures, there are only a few strong spots in the diffraction patterns combined with several extinctions or very weak spots. The weak reflections, although they were taken into account, will not, or only very slightly, contribute to the statistical averages concerning only the power of the normalized structure factor (the first six values in Table 3) but will affect the other two. The array sizes for the simulations are 32×32 for copper, 64×64 for silicon and silicon dioxide and the samplings of the projected unit cells are 0.113 by 0.113 Å, 0.085 by 0.085 Å and 0.111 by 0.111 Å, respectively.

The S_{area}s used for these three structures are chosen according to the positions of their strong reflections. For example, for silicon dioxide, the strong reflections inside a circle of 1.2 Å^{-1} are indexed as 220, 400, 440, 620, 800 and 660, which correspond to 0.399, 0.564, 0.798, 0.892, 1.128 and 1.196 Å^{-1}, respectively. Therefore, S_{area}s of 1.20, 1.13 and 0.90 Å^{-1} are applied to this structure. Similarly, S_{area}s are 1.24, 1.11 and 0.79 Å^{-1} for copper and 1.17, 1.05 and 0.74 Å^{-1} for silicon.

Fig. 4 shows the thickness determined by the technique *versus* the thickness actually used in the diffraction calculation (true thickness or T_{true}) for three different S_{area}s as labelled in the figure for copper. A

smaller S_{area} of 0.56 Å^{-1} contains only 200 reflections and always gives the determined thickness $T_{det} = 0.0$, which leads to no improvement so this S_{area} is ignored.

Fig. 5 gives the R factors before (a) and after (b, corresponding to Fig. 4) for three S_{area}s. The former is denoted as R_o and the latter as R. R_o represents an R factor calculated directly from the diffraction and the structure factor and is also equivalent to that obtained from a set of restored data with $T_{det} = 0.0$. The R factor is defined as

$$R = \sum_{\mathbf{g}} \big||F(\mathbf{g})| - k|F'(\mathbf{g})|\big| \Big/ \sum_{\mathbf{g}} |F(\mathbf{g})| \qquad (10)$$

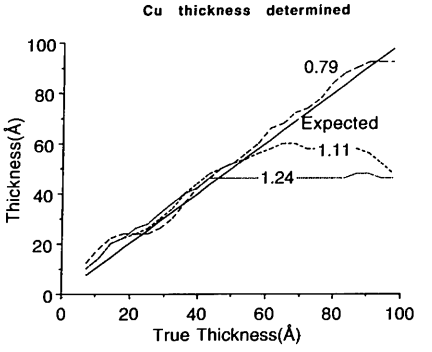

Fig. 4. The thickness determined by the restoration technique with three different S_{area}s for copper compared with the expected thickness.

with scaling factor

$$k = \sum_{\mathbf{g}} |F(\mathbf{g})F'(\mathbf{g})| \Big/ \sum_{\mathbf{g}} |F'(\mathbf{g})|^2. \qquad (11)$$

It is clear and impressive from Fig. 5 that the technique results in a set of better structure-factor moduli than the diffraction itself, with the much improved R factors after restoration.

The estimated thickness is in good agreement with the true thickness for all the S_{area}s except in the cases where the thickness limit is approached or surpassed. For larger S_{area}s, the deviation from the theoretical expected diagonal line begins sooner because of its smaller thickness limit. Therefore, it is easy to accept the T_{det} with the smallest possible size. However, it should be noted that there are 20 strong reflections within a circle with a radius of 1.24 Å^{-1}, while inside 0.79 Å^{-1} there are only 8. Apart from the better statisitics, we would also like to have as many reflections modified as possible. Therefore, to make things more general and more accurate, the largest possible S_{area} should be chosen unless its determined thickness is smaller than that from a smaller S_{area} with a smaller $M(T_{det})$.

Accordingly, Fig. 6 shows both (a) the determined thickness and (b) R_o and R for silicon. The S_{area}s used have been switched from 1.17 to 1.05 Å^{-1} around $T_{true} = 60$ Å and switched again to 0.74 Å^{-1} around 80 Å true thickness. The switch points are clearly seen in

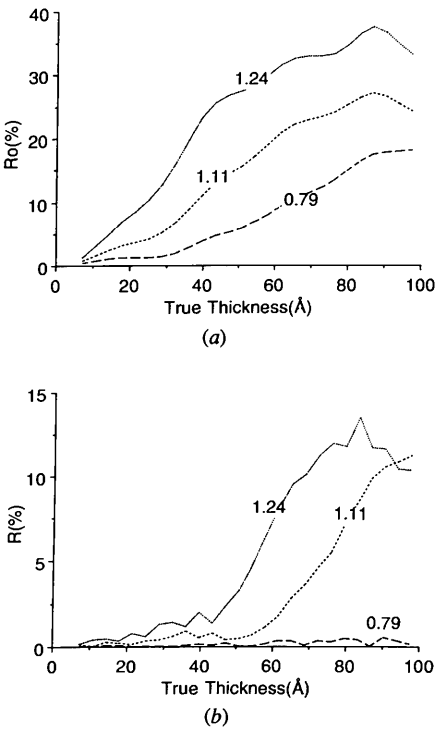

Fig. 5. The R factors (a) before and (b) after restoration for copper.

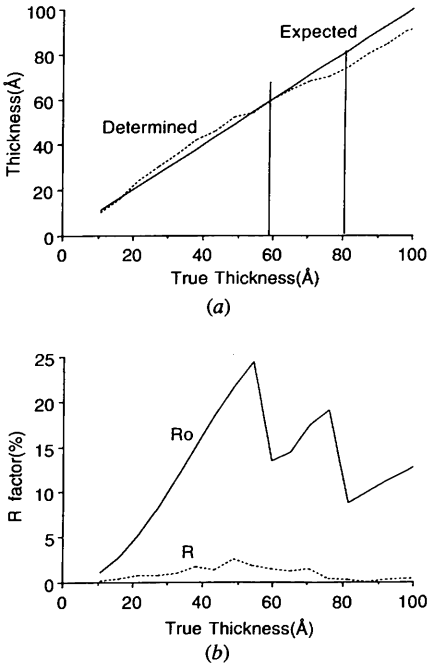

Fig. 6. (a) The determined thickness values and (b) the R factors for silicon. The S_{area} used for the determined thickness curve has been switched from 1.17 to 1.05 Å^{-1} and then to 0.74 Å^{-1} at the thickness indicated by the two vertical lines in (a).

Fig. 6(*b*) when R_o has a quite different value; these points are indicated in Fig. 6(*a*) by the vertical lines.

Fig. 7 is another example of simple structure-factor-modulus restoration for silicon dioxide. There is no S_{area} switch because $1.2\,\text{Å}^{-1}$ gives a bigger, and closer, determined thickness than those obtained for $1.13\,\text{Å}^{-1}$. The S_{area} of $0.9\,\text{Å}^{-1}$ is ignored since T_{det} is always zero even though there are still 20 diffraction spots. R and R_o are also shown in the figure. The figure gives the results beyond the thickness limit (66 Å) with far smaller T_{det} than T_{true} but still with an improved R factor.

All the above tests are achieved with the non-centrosymmetric statistical values, but switching to the centrosymmetric statistics did not lead to different T_{det} and relative $M(T_{det})$ values.

3.4. *Test of a complicated structure*

The restoration of a complicated structure with a large unit cell and many more atoms, zeolite-L ($Al_{36}Si_{36}K_{14}O_{71}$) along the [001] direction (Breck, 1974), has been investigated. Zeolite-L is hexagonal with $a = 18.466$ and $c = 7.476$ Å. The array size is 66×66, corresponding to a sampling of 0.2798 by 0.2798 Å. Because of the large size of the unit cell compared with the above simple structures, the diffraction patterns contained many significant reflections. Within $1.2\,\text{Å}^{-1}$ in reciprocal space, there are over 1300 reflections for the zeolite whereas there are only 28 reflections for silicon dioxide. Choosing S_{area} according to the positions of all reflections, a trick used for the simple structures to simplify the calculation, is certainly not applicable owing to the number of reflections. Instead, S_{area} is chosen uniformly with the fine increment of $0.01\,\text{Å}^{-1}$, starting from the largest possible S_{area} until T_{det} decreases. Fig. 8 shows such T_{det} and $M(T_{det})$ curves against the radius of S_{area} for $T_{true} = 37.38$ Å (*a*) and 52.33 Å (*b*), respectively. T_{det} ranges from 24 to 96 Å for the former and from 44 to 76 Å for the latter according to the various radii. According to the criterion we used in the last section, the T_{det}s are 44 and 54 Å for these two true thicknesses at $S_{area} = 1.18\,\text{Å}^{-1}$ because there is no larger T_{det} with smaller $M(T_{det})$ when $S_{area} < 1.18\,\text{Å}^{-1}$.

Although with this very fine increment of S_{area} and by monitoring the change of merit factor $M(T_{det})$, a best T_{det} and then a best set of $|F'|$ can be picked up, this needs a long time and many calculations. Therefore, another approach, restricting some strong reflections as outlined below, is more appropriate. The scrutiny of T_{det} curves suggests that it changes with the radius of S_{area} not continuously but jumping at certain values. These radii correspond to some of the strongest reflections in the diffraction pattern. For example, in Fig. 8(*a*), T_{det} curves jump at 1.18, 1.08, 0.99 and 0.94 to $0.93\,\text{Å}^{-1}$, which correspond to the five strongest reflections 0,19,0, 10,10,0, 6,12,0, 240 and 6,11,0 in the region from 0.9 to $1.2\,\text{Å}^{-1}$. At the same positions, $M(T_{det})$ changes more or less sharply. The strong reflection with large g value is generally disadvantageous, because it either violates the kinematical conditions at a smaller thickness than the weak reflections (Vainshtein, 1964) or reaches its thickness limit earlier than the reflection with smaller g value. Excluding it could be better for the technique. A possible simplified method for this complicated structure could be that only the largest possible radius and those radii of S_{area} just excluding a strong reflection are used.

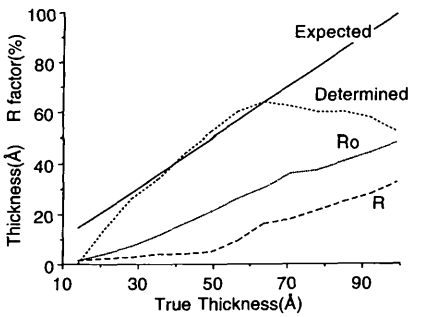

Fig. 7. The determined thickness and R factors before (R_o) and after (R) restoration for silicon dioxide The thickness region greater than the thickness limit is also plotted, where although the determined thickness is far less than the expected one the R factor is still improved.

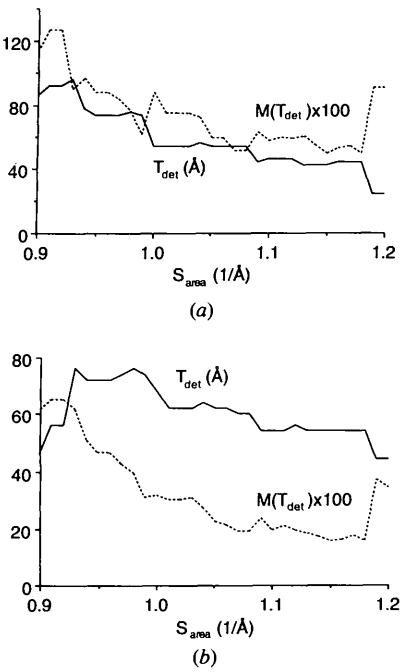

Fig. 8. The changes of T_{det} and $M(T_{det})$ against S_{area} for zeolite-L at (*a*) $T_{true} = 37.38$ Å and (*b*) 52.33 Å. T_{det} does not change continuously but jumps step by step at the positions of the strongest reflections.

Table 4. *The determined thickness, its deviation from the true thickness, the radius of S_{area} used for obtaining the determined thickness, the initial R value and the improved R values for 36 to 48 strongest reflections within an annular area from 0.4 Å^{-1} to the corresponding radius for zeolite-L*

T_{true} (Å)	T_{det} (Å)	$\|T_{true} - T_{det}\|$	Radius (Å^{-1})	R_o (%)	R(%)
14.95	50 (38)	45.05 (23.05)	1.18 (1.20)	1.16	
22.43	48 (34)	25.57 (11.57)	1.18 (1.20)	2.87	
29.90	44 (26)	14.10 (3.90)	1.18 (1.20)	6.60	(4.15)
37.38	44	6.62	1.18	15.86	6.50
44.86	48	3.14	1.18	30.01	16.19
52.33	54	1.67	1.18	36.92	18.58
59.81	62	2.19	1.08	27.74	8.62
67.28	62	5.28	0.99	15.47	9.17
74.76	66	8.76	0.88	21.65	14.78
82.24	90	7.76	0.81	31.30	18.93
89.71	106	16.39	0.81	40.71	24.85

Based on this idea, the selected radii of S_{area} for $T_{true} = 52.33$ Å are 0.93, 0.94, 1.00, 0.99, 1.08, 1.18 and 0.98 Å^{-1}, in order of intensity, and 1.2 Å^{-1}, and the recognizable T_{det} jumps are at 0.93, 1.0–0.98, 1.08 and 1.18 Å^{-1}, obeying the rule we have outlined.

Accordingly, tests here made for different T_{true} from 14.95 to 89.17 Å and the result is shown in Table 4. When $T_{true} \leq 29.90$ Å, the technique gives T_{det} far from T_{true}, for example $T_{det} = 48$, for $T_{true} = 22.43$ Å, with error of more than 110%. At the same time. $M(T_{det})$ becomes much bigger than others with a small error in T_{det}, say more than three times. However, this deviation is not important either because the experimental diffraction from this small-thickness region is difficult to obtain or because the crystal is so thin that such restoration is not needed, which is clearly shown in Table 4 by the small R_o value at the small thickness and is also indicated in Fig. 3. A slightly better T_{det} can be obtained using the biggest possible radius of S_{area}. These T_{det}s are also shown in Table 4 within parentheses, in which the largest possible radius of S_{area} of 1.2 Å^{-1} is used. The relative error of T_{det} reduces from more than 110 to 52% for $T_{true} = 22.43$ Å. The reason for the huge error arising from the small thickness will be discussed later.

The R factors before and after restoration, calculated with $|E'|$ rather than $|F'|$, are also listed in Table 4. Several strongest structure factors within an annular area, from 0.4 Å^{-1} to a radius consistent with one used in T_{det} calculation and listed in column Radius, have been chosen for R calculation. (The overall R factor, full area and all the reflections, does not always reduce. The reason is not very clear and is being investigated.) The R factor is not improved for the two smallest thickness values, arising from the huge difference in the determined thickness. The effect of dynamical scattering is reflected by the increase of R_o with the thickness. Despite this inevitable dynamical effect, the R factors are greatly reduced. In the best case, the new R factors is less than a third of the old one.

3.5. *Test on a structure with relatively heavy elements*

Because of the kinematical condition for the validity of (1), structures with only light elements are ideal for testing, otherwise the kinematical condition could be violated with the increase of thickness. All the above test structures are in this category, without an atom heavier than copper. In this section, the specimen of $NdSr_2NbCu_2O_8$ along the [010] direction, which contains the medium-heavy elements Nd ($Z = 60$), Nb ($Z = 41$) and Sr ($Z = 38$), is once again under investigation. Although the unit cell ($a = b = 3.88$, $c = 11.75$ Å) is not as big as zeolite; because of the lower symmetry there are still many reflections with significant intensity in the diffraction pattern. Within a 1.2 Å^{-1} circle, there are more than 200 reflections, an advantage for statistics.

The procedure used for this material is exactly the same as for zeolite-L: only the largest possible g and those just excluding one of the strongest reflections are chosen to be the radii of S_{area}. The huge error in T_{det} also occurs at the small thickness. It is impossible to improve it with the larger S_{area} as in the case of zeolite because the best S_{area} is 1.2 Å^{-1}. However, if we exclude a few strongest reflections in the diffraction pattern, which is equivalent to increasing the influence of numerous less-strong reflections to the statistics, and monitor the change of the merit factor, the result is considerably improved. For example, for $T_{true} = 19.40$ Å, the new T_{det} is 10 Å instead of 36 Å. For this specimen, this second cycle of calculation only works for T_{true} less than 34 Å. Beyond this thickness, no further improvement is obtained with exclusion of the strongest reflections.

Fig. 9 shows the determined thickness, the expected thickness and the R factors. The second-cycle calculation is included so that the error at $T_{true} < 34$ Å is reasonably small. Although there are heavy elements in the structure, this technique still gives acceptable T_{det} values up to the thickness suitable for experiment, although R is not as small as that for silicon dioxide in Fig. 7.

It must be mentioned that the same second-cycle calculation has also been applied to zeolite and the

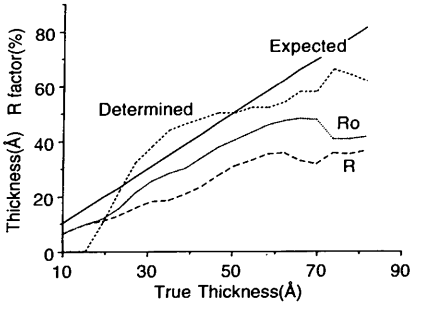

Fig. 9. The curves show the determined thickness, the expected thickness and the improvement of R factors with the different true thicknesses for $NdSr_2NbCu_2O_8$.

simple structures, but no further improvement can be made based on the M factor.

4. Discussion

The kinematical approach for thickness determination and restoration of the structure-factor modulus from electron diffraction patterns has been tested and it has been shown that it is working under some restrictions. Firstly, the function $D(s_g t)$ is based on kinematical scattering theory and thus the thickness of the specimen is limited to near-kinematic conditions. This restricts the thickness of the crystal depending on the weight of the constituent elements. Secondly, when the crystal is too thin, the approach gives rise to a relatively large error in the determined thickness and restoration.

Both small thickness and small S_{area} lead to relatively large errors. For small T_{true}, the argument of the shape function $s_g t$ is near to zero so that the value of the shape function is almost unity everywhere. The differences among arguments for different trial thicknesses and also among these for different reflections at the same trail thickness are also close to zero. All of these cause the error in thickness determination because, from (6), the magnitude of $|F'|$ will not vary prominently if the shape function is not very different.

The differences among arguments are further reduced if only small S_{area}s or small s_gs are considered. the small S_{area} also reduces the number of reflections included in the statistical calculation, a setback for statistics. Therefore, as large as possible an S_{area} has been used in the above tests as long as the thickness limit permits. Theoretically, a smaller S_{area} can be used in the thicker region where the disadvantages of a small S_{area} are compensated for by the large thickness value, as shown in all the cases above.

As illustrated in Table 4 for zeolite, where the thickness difference $|T_{\text{true}} - T_{\text{det}}|$ has a minimum value around $T_{\text{true}} = 50$ Å, the best thickness estimation is made in the region neither too thin nor too thick. The large thickness increases the precision of the statistics. However, since the technique is based on the kinematical condition, an over-thick specimen (where the dynamical effect cannot be so simply ignored) will certainly lead to a less-reliable result.

The thickness limit for an individual S_{area} owing to an over-small value of the shape function is a disadvantage in this technique. If there were no such limitation, T_{det} could be obtained after only one calculation with the largest possible S_{area} and with as many reflections as possible. An approximation that we tried, setting $D(s_g t)$ to be, for instance, 0.05 for all the reflections with $D(s_g t) < 0.05$ and including them into the statistics so that only one S_{area} is needed, did not give a successful result. A possible experimental solution to the problem caused by $D(s_g t) < 0.05$ is perhaps to deliberately converge the electron beam a little, causing the shape function to be a sum of a few sinc functions with the principal maxima locating around $s_g = 0$. In doing so, the minimum value of the new shape function is possibly always greater than 0.05. At the same time, (6) must be rewritten and the sinc function must be replaced by a group of sinc functions.

Apart from the thickness and the atomic number of the constituent elements, another factor affecting the precision of the technique is the number of different elements in a unit cell. Because the statistics of Table 3 are based on a single-element structure, any other elements will cause deviations from the theoretical data. Perhaps this is why, in the simple structure tests, restoration can be achieved for both copper and silicon up to 100 Å while it is only valid for silicon dioxide to 60 Å. This restriction may be partly counteracted by increasing the number of reflections, as in the case of zeolite and $NdSr_2NbCu_2O_8$, which have four and five different elements, respectively, some much heavier than silicon, but can still be processed over 60 Å.

Unlike the simple structures, only non-centrosymmetric statistical values in Table 3 are successfully used for both zeolite and $NdSr_2NbCu_2O_8$, although their structures are centrosymmetric. The structure-factor statistics predict that the probability distribution function of the magnitude $|E|$ has a maximum either at zero for centrosymmetric or at $2^{-1/2}$ for non-centrosymmetric structures (Karle, 1972). For the simple structures, because the number of reflections is so small, the distribution of $|E'|$ has no apparent maximum so that both statistics worked. For the other structures we encountered, Wilson statistics have been done using the *NORMAL* program (Wilson, 1942; Main, 1985) and the distribution of $|E|$ was then assessed. The distribution of $|E'|$ was close to the non-centrosymmetic one so that these statistics were more appropriate.

The remaining question is why only non-centrosymmetric statistics are successful while the structures investigated have centres of symmetry. The reason is not completely clear. The most probable reason is perhaps from the statistical error. The average actually made is different from the statistical theory in the following aspects: there is more than one constituent element in the structure; the reflections are not uniformly distributed in reciprocal space; the average has been done in two dimensions rather than three dimensions *etc.* All of these could lead to the deviation of averages from the theoretical values. In fact, in X-ray theory, the statistical values given in Table 3 will also deviate slightly from different space groups. The question is subject to further research.

Whereas for structures with only low-scattering-power elements the scattering is close to kinematical, for crystals with heavy elements it is only a rough approximation. The kinematical condition is only valid for small thickness depending on the weight of the composition. However, all the above tests showed that

utilization of the kinematical formula can be extended to a thickness much beyond the thickness where only kinematical diffraction has to be considered, for example 100 Å for an element as heavy as copper or 70 Å for crystals with medium-heavy elements like Nd. This is because at the first stage of dynamical scattering the diffraction amplitude is still close to the structure-factor modulus while the phase of it begins to deviate (Dorset, Tivol & Turner,1992), as we mentioned at the beginning of the paper. It ensures that the kinematical structure-factor restoration is usable to a practical thickness, say several nanometres. As mentioned above, the best working thickness is neither too thin nor too thick. For structures without very heavy elements, this is well within the experimentally available region. It is one of the most important results of this study that the crystal thickness may be estimated from the electron diffraction pattern, perhaps with less than 10% error under the best conditions for very complicated structures.

The study reported in this paper is the starting point of a more extensive and more realistic study of the structure-factor-modulus restoration under dynamical conditions, as Dorset (1992) and Sha, Fan & Li (1993) have attempted in limited cases previously. The accuracy of the method in this kinematical approach is greatly restricted by the thickness and the weight of the elements. These restrictions will be reduced if the dynamical effect is taken into consideration. The importance of this study is that the normalized structure-factor statistics can be employed for assessment, which could be a potential future tool under dynamical conditions. Tests including the dynamical effect are being performed at the moment.

5. Concluding remarks

It is possible to estimate the crystal thickness and improve the kinematical electron diffraction intensities to obtain a set of data closer to the structure-factor moduli by dividing them by the square of a sinc-type shape function, thus correcting for the curvature of the Ewald sphere.

For theoretical image calculation, the paraboloidal approximation to the spherical wave front in the Fresnel propagator is generally acceptable, with no more than 1% difference even for a relatively thick specimen.

The theoretical tests show that, at a thickness near kinematical conditions (up to 70–100 Å), the specimen thickness can be estimated with reasonably small error and the diffraction data can be processed to produce a set of data closer to the structure-factor modulus even for relatively complicated structures and structures with medium-heavy elements.

The thickness determination and the application of the structure-factor statistics are two major results of this study, which is useful for the future possible dynamical scattering correction and the structure-factor restoration under dynamical conditions.

The authors would like to acknowledge the STW for a Research Fellowship.

References

BALDWIN, J. & HENDERSON, R. (1984). *Ultramicroscopy*, **14**, 319–336.

BRECK, D. W. (1974). *Zeolite Molecular Sieves*, p. 156. New York/London/Sydney/Toronto: John Wiley.

COWLEY, J. M. (1988). In *High-Resolution Electron Microscopy*, edited by P. R. BUSECK, J. M. COWLEY & L. EYRING, p. 72. Oxford Univ. Press.

COWLEY, J. M. & MOODIE, A. F. (1957). *Acta Cryst.* **10**, 609–619.

DONG, W., BAIRD, T., FRYER, J. R., GILMORE, C. J., MCNICOL, D. D., BRICOGNE, G., SMITH, D. J., O'KEEFE, M. A. & HOVMÖLLER, S. (1992). *Nature (London)*, **355**, 605–609.

DORSET, D. L. (1992). *Acta Cryst.* A**48**, 568–574.

DORSET, D. L., TIVOL, W. F. & TURNER, J. N. (1992). *Acta Cryst.* A**48**, 562–568.

DOWNING, K. H., MEISHENG, H., WENK, H. R. & O'KEEFE, M. A. (1990). *Nature (London)*, **348**, 525–528.

FAN, H., ZHONG, Z., ZHENG, C. & LI, F. (1985). *Acta Cryst.* A**41**, 163–165.

GIACOVAZZO, C. (1980). *Direct Methods in Crystallography*. London: Academic Press.

GOODMAN, P. & MOODIE, A. F. (1974). *Acta Cryst* A**30**, 280–290.

HU, J. J., FAN, H. F. & LI, F. H. (1992). *Ultramicroscopy*, **41**, 387–397.

ISHIZUKA, K., MIYAZAKI, M. & UYEDA, U. (1982). *Acta Cryst.* A**38**, 408–413.

KARLE, J. (1972). *Acta Cryst.* B**28**, 3362–3369.

KILAAS, R., O'KEEFE, M. A. & KRISHNAN, K. M. (1987). *Ultramicroscopy*, **21**, 47–62.

LIU, Y., XIAN, S., FAN, H., TANG, D., LI, F., PAN, Q., UYEDA, N. & FUJIOSHI, Y. (1990). *Acta Cryst.* A**46**, 459–463.

MAIN, P. (1985) *Crystallographic Computing* 3, edited by G. M. SHELDRICK, C. KRÜGER & R. GODDARD, pp. 206–215. Oxford: Clarendon Press.

PINSKER, Z. G. (1953). *Electron Diffraction*, p. 89. London: Butterworths.

SHA, B. D., FAN, H. & LI, F. (1993). *Acta Cryst.* A**49**, 877–880.

TANG, D. & LI, F. H. (1988). *Ultramicroscopy*, **25**, 61–68.

VAINSHTEIN, B. K. (1964). *Structure Analysis by Electron Diffraction*, pp. 148–151. Oxford: Pergamon Press.

WELLS, A. F. (1954). *Structural Inorganic Chemistry*, p. 464. Oxford: Clarendon Press.

WILSON, A. J. C. (1942). *Nature (London)*, **150**, 151–152.

ZANDBERGEN, H. W., CAVA, R. J., KRAJEWSKI, J. J. & PECK, W. F. JR (1993). *J. Solid State Chem.* **101**, 322–325.

ZOU, X. D., HOVMÖLLER, S., PARRAS, M., GONZÁLEZ-CALBET, J. M., VALLET-REGÍ, M. & GRENIER, J. C. (1993). *Acta Cryst.* A**49**, 27–35.

ZOU, X., SUKHAREV, Y. & HOVMÖLLER, S. (1993). *Ultramicroscopy*, **49**, 147-158.